Sea-Thru Overview

Jaskarandeep Singh
Thapar Institute to Engineering Technology
Patiala,Punjab,India
Jsingh6_be20@thapar.edu

Ankur Garg
Thapar Institute to Engineering Technology
Patiala,Punjab,India
Agarg8_be20@thapar.edu

Manvi Mehendiyan
Thapar Institute to Engineering Technology
Patiala,Punjab,India
Mmehendiyan_be20@thapar.edu

Abstract

Recovery of lost colours from underwater images has always been a challenging task. And there had always been a need for one for discovering underwater life and the world. This model shows 1)the attenuation coefficient in presence of water is related to wavelength, reflectance and distance between the object and camera lens, and is not uniform all across the scene. 2)The backscatter coefficient is dependent on the distance between the object and the camera lens(z). And increases with z. 3)This is the first method that recovers colour using a revised image generation model, using RGBD images 4) It uses a range-dependent attenuation coefficient for the estimation of spatially varying illumination.

This model uses more than 1100 images from two optically different waterbodies and our revised model consistently removes water from images, creating exciting opportunities for the discovery and future of underwater exploration.

1. Introduction

Reconstructing the image's colour underwater has always been challenging despite consistent development in the field of cameras. For this, there is still a need for a robust algorithm. As AI-powered underwater vehicles with visualising sensors because of their attractive and energy efficient and human-safe nature. So we can discover the depths of oceans without endangering the life of Humans but underwater imagery has not fully benefited from Machine Learning and Computer Vision, as it consists of many computational challenges and the image taken in water is equivalent to an image taken in air and covered in coloured fog with illuminations. An approach towards a solution to this issue is to be able to restore the images such that they appear in the air(in absence of water), i.e., with corrected colours and suspended particles removed from the scene

But as for now some of the algorithms that have been developed and show pretty good results, known as the Underwater Generative Adversarial Networks, developed by the University of Minnesota, Minneapolis MN which was later replaced by a better algorithm known as the Sea-thru method developed by Derya Akkatanak and Tali Treibitz.

Sea-thru is a physics-based colour reconstruction algorithm designed for underwater RGB-D images.

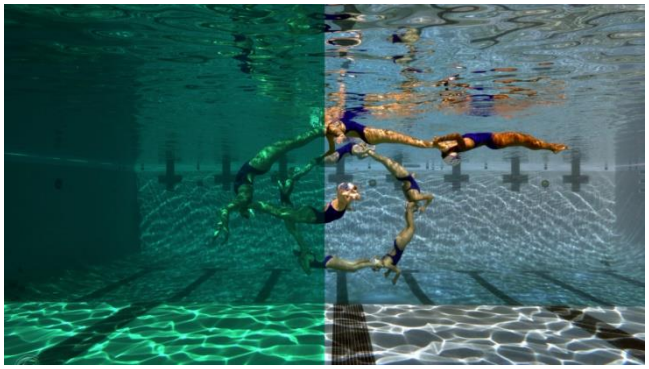

It is a non-deep learning-based algorithm developed in 2019 and is still the best algorithm.

The Underwater image generation is controlled by the equation, **Ic = Dc + Bc**.
Dc contains the scene with attenuated colours, and **Bc** is a degrading signal that strongly depends on the optical properties of the water.

2. Related Work

The image creation model for bad weather was developed by Nayar and Narasimhan. In this algorithm the scattering coefficient was assumed to be constant over the camera's sensitivity range for RGB channel, which results in a coefficient per wavelength, this method was further used in underwater imagery for attenuation coefficient, and the backscatter coefficient was estimated by DCP (dark channel prior) which removes haze from the input image. The attenuation constant can be measured with the help of ocean optic instruments but to achieve an economical system this attenuation constant was calculated directly from the image with the help of physics equations in the Sea thru method.

3. Scientific Background

Underwater water images follow the equation of light:

Ic = Dc + Bc , (1)
The components Dc and Bc depend on wideband attenuation and backscatter coefficients, respectively [1, 2].

(Here the Forward scatter signal is ignored since it is negligible in an underwater scene).

where c = R,G,B is the colour channel, Dc is the direct signal and

Bc is the *backscatter* signal.

The expanded form of Eq. 1 is given as [1]:

$$I_c = J_c e^{-\beta_c^D(\mathbf{v}_D)\cdot z} + B_c^\infty \left(1 - e^{-\beta_c^B(\mathbf{v}_B)\cdot z}\right) \quad , \qquad (2)$$

Eq. 2 is applied in all directions assuming that the deviation for different directions is very small

where z is range between the camera and the objects, B_c^∞ is veiling light, and Jc is the scene excluding attenuation

$\mathbf{v}_D = \{z, \rho, E, S_c, \beta\}$ and $\mathbf{v}_B = \{E, S_c, b, \beta\}$.

represent the dependencies of the coefficients on range z, reflectance rho, spectrum of ambient light E, spectral response of the camera Sc,

and the physical scattering and beam attenuation coefficients

of the water body, b and β, all of which are functions of wavelength.

Previously, it was assumed that wideband attenuation and backscatter coefficients were constant for a particular scene [9], but in [1] we see that they are distinct and have discrete dependencies.

The equations connecting RGB coefficients β_c^D and β_c^B to wavelength dependent physical quantities are [1]:

$$\beta_c^D = \ln\left[\frac{\int_{\lambda_1}^{\lambda_2} S_c(\lambda)\rho(\lambda)E(d,\lambda)e^{-\beta(\lambda)z}d\lambda}{\int_{\lambda_1}^{\lambda_2} S_c(\lambda)\rho(\lambda)E(d,\lambda)e^{-\beta(\lambda)(z+\Delta z)}d\lambda}\right] \Big/ \Delta z \ , \qquad (3)$$

$$\beta_c^B = -\ln\left[1 - \frac{\int_{\lambda_1}^{\lambda_2} S_c(\lambda)B^\infty(\lambda)(1-e^{-\beta(\lambda)z})d\lambda}{\int_{\lambda_1}^{\lambda_2} B^\infty(\lambda)S_c(\lambda)d\lambda}\right] \Big/ z \ . \qquad (4)$$

Here, λ_1 and λ_2 are the limits of the visible range (400 and 700nm), E is the spectrum of ambient light at depth d. Light penetrating vertically attenuates based on the *diffuse downwelling attenuation* $K_d(\lambda)$ [47], different than the beam attenuation coefficient $\beta(\lambda)$ [1, 47] which is solely a function of the type, composition, and density of dissolved substances in the ocean [47]. If $E(0,\lambda)$ is light at the sea surface, then $E(d,\lambda)$ at depth d is [2]:

$$E(d,\lambda) = E(0,\lambda)e^{-K_d(\lambda)d} \ . \qquad (5)$$

The veiling light B_c^∞ in Eq. 2 is given as:

$$B_c^\infty = \int_{\lambda_1}^{\lambda_2} S_c(\lambda)B^\infty(\lambda)d\lambda \ , \qquad (6)$$

where

$$B^\infty(\lambda) = \left[b(\lambda)E(d,\lambda)\right]/\beta(\lambda) \ . \qquad (7)$$

4. The Sea-Thru Method

Based on Eqs. 2-4, to recover the unattenuated scene the following need to be estimated: optical water type; light Ed, z, depth at which the photo was taken d, the reflectance of each object,
and the spectral response of the camera Sc.
we estimate the relevant parameters for a
given image from that image only.We tailor the sea thru method.

to tackle the dependencies listed above in the scientific background.

4.1. Imaging and Range Map Generation

The wideband (RGB) attenuation coefficient, β^D_c is dependent on z. That is why we need to have a range map which contains the distances of the point in the scene to another point. This point here is the camera's position. The Range map here is obtained using structure-from-motion (SFM), which is the photogrammetric range imaging technique for estimating 3D structures from 2D image sequences. Our model needs an absolute value for z but SFM gives range only up to scale, so we have kept a color chart (Fig) with the object in the images to set the scale.

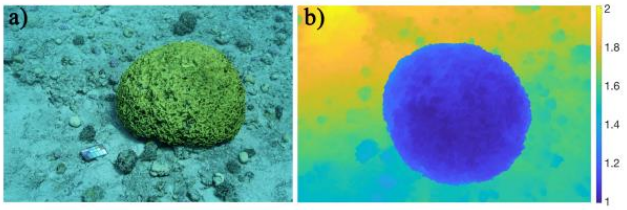

Figure 3. **a)** A 3D model created from 68 photographs using Photoscan Professional (Agisoft LLC). **b)** Range map z (in meters) for the image in Fig. 1 obtained from this model. We placed a color chart on the seafloor to set the scale.

4.2. Scene Reconstruction

From Eqs. 1 & 2 we have:

$$J_c = D_c e^{\beta_c^D(z)z}$$

where $D_c = I_c - B_c$. Here we are ignoring all the other dependencies except for z dependency of wideband (RGB) attenuation coefficient. Here J_c is an image whose colors are only corrected along z; it will take further computations to get an image equivalent to what was taken at sea surface.

$$J_s = J_c / W_c$$

Here J_s is the image taken at the sea surface, W_c is the white point of the ambient light at the camera at depth d.

4.3. Backscatter Estimation

As we increase z, backscatter increases exponentially and eventually the image saturates. Where scene reflectance $\rho_c \to 0$ (all light absorbed), or $E \to 0$ (complete shadow), the captured RGB intensity $I_c \to B_c$. We will look for very dark or shadowed pixels in the image and then use these pixels to get an initial estimate of backscatter. It basically tries to find the backscattered signal where the D_c is minimum, we utilize a known range map for it. Additionally, we search for the darkest RGB triplets. The small number of unconnected pixels our method identifies is sufficient, because we have

the corresponding range information, and a physical model of how B_c behaves with z.

To estimate backscatter, we use the following step: first we partition the given range map into 10 evenly spaced clusters spanning the minimum and maximum values of z. In each range cluster, we search I_c for the RGB triplets in the bottom 1 percentile, which we denote by **Ω**. Then across the whole image, is an overestimate of backscatter. $\hat{B}_c(\Omega) \approx I_c(\Omega)$

Fig demonstrates this method, where the veiling effect of backscatter due to decrease in z i.e., the distance between the camera and the chart is clearly visible.

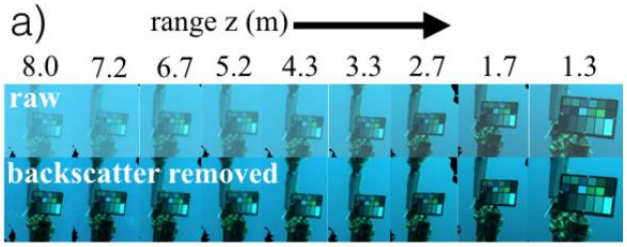

Fig The top row show the raw images I_c, the bottom row shows the corresponding Dc or the backscatter-removed images.

4.4. Attenuation Coefficient Estimation

4.4.1 β_c^D as a Function of z

We previously showed that β_c^D varies with range z [1, 2] in the form of exponential decay we first describe the relation between β_c^D and z.

$$\beta_c^D(z) = a * \exp(b * z) + c * \exp(d * z) \ .$$

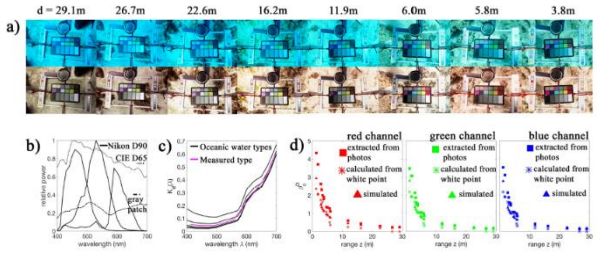

Figure 5. Using a dataset from [2] we calculate $\beta_c^D(z)$ in three different ways: extracting it from photos of the same object at two different distances; calculating it using the white point of the ambient light using Eq. 9; and simulating it using Eq. 3.
a) Raw images captured by the camera
b),c),d) are the three methods listed

4.4.2 Coarse Estimate of $\beta_c^D(z)$ From an Image

We now proceed to estimating $\beta_c^D(z)$
The recovery of scene Jc reduces to
a problem of the estimation of the spatially variable $\hat{E}_c(z)$ local illumiant map

$$\hat{\beta}_c^D(z) = -\log \hat{E}_c(z)/z.$$

Here, we use a variant of the LSAC method [24]:
for a given pixel (x, y) in color channel c, local space average color ac(x, y) is estimated iteratively.

$$a'_c(x,y) = \frac{1}{N_e}\sum_{N_e} a_c(x',y')$$

$$a_c(x,y) = D_c(x,y)p + a'_c(x,y)(1-p) \ ,$$

4.4.3 Refined Estimate of $\beta_c^D(z)$

From coarse equation defined:

$$\hat{z} = -\log \hat{E}_c/\beta_c^D(z) \ ,$$

Further,

$$\min_{\beta_c^D(z)} \|z - \hat{z}\|,$$

5. Dataset

The Dataset used for the Sea-Thru training consists of five underwater **RGBD** (red, Green, Blue and Depth) datasets. Which were all taken in **natural illumination** and in **Raw format** (an image that is minimally processed and is saved without compressing) with contrast depending on the dataset selected, these contain multiple images with colour charts with them.

5.1.1. Subsubsections

The heading for subsubsections should be in Times New Roman 10-point italic with initial letters capitalized and 6 points of white space above the subsubsection head.

6. Results and Error Analysis

The scenarios followed by the former model (2019 Sea-Thru) are:

S1. Contrast Stretching.

S2. Estimation of Backscatter coefficient (B_c) using DCP (Dark Channel Prior), which is implemented by the *imreducehaze* function in our code.

S3. Model With corrected estimation for Backscatter and assuming $\beta_c = \beta^D_c = \beta^B_c$.

S4. Corrected estimation for Backscatter (B_c) coefficient and Unsaturated Scene (J_c), uses $J_c = D_c/E_c$, without calculating β^D_c (z).

S5. The Revised Model doesn't consider Backscatter Coefficient (B_c) and Direct Signal Coefficient (D_c) to be the same and shows the dependency of Z (distance between the camera and the object) on the Direct Signal Coefficient (D_c).

Sea-Thru is the first algorithm produced using a revised underwater image formation model and thus has the advantage of using Range maps. Based on one of the surveys on DCP, authors found that Models using DCP were not able to consistently produce corrected colours, whereas other models were good for producing enhanced images but failed to produce physically accurate corrections.

The Proposed method aims to generate physically accurate colours but only works for horizontal imaging with sufficiently large distances in the scene, thus making our model less suitable for most of the scenarios.

The following images show results after using S1-S5 on the input images(D1-D5) in Stereo Database.

For evaluation purposes RGB angular error $\bar{\psi}$ (for 6 different grayscale patches).

$$\bar{\psi} = (1/6)\cos^{-1}[I_c/(\sqrt{3}.\| I_c \|)]$$

(Lower the Value of $\bar{\psi}$, Better the Colour Correction)

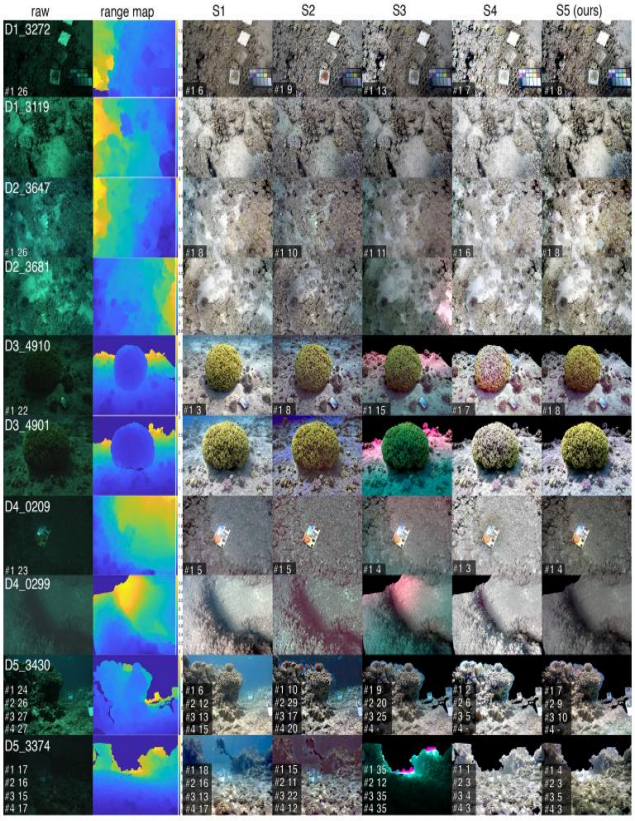

Figure 6. Results on **D1-5** (Table 1). For each chart and method, $\bar{\psi}$ rounded to the nearest integer is given in inset; Chart #1 is closest to the camera. Average errors for the dataset are: **raw:** 20.57, **S1:** 12.49, **S2:** 14.38, **S3:** 21.77, **S4:** 4.13, **S5:** (*Sea-thru*) 6.33.

In these cases,

S1 – works well when scene distances are approximately uniform.

S2 – DCP-based estimation often overestimates backscatter (can improve visibility), causing images to be distorted and have hallucinated colours. The grey patch of the colour chart has visible purple artefacts

S3 – Attenuation is corrected with a constant $\beta^D{}_c$. the incorrect assumption for constant $\beta^D{}_c$ is visible when there is a large variation in the range map. It also fails for the scenes with comparatively shorter ranges.

S4 – After correcting the estimations for Backscatter and direct light, it sometimes shows lower error than S5, whereas S5 results better in complete scenes. Thus, S4 can be used for the first-order correction.

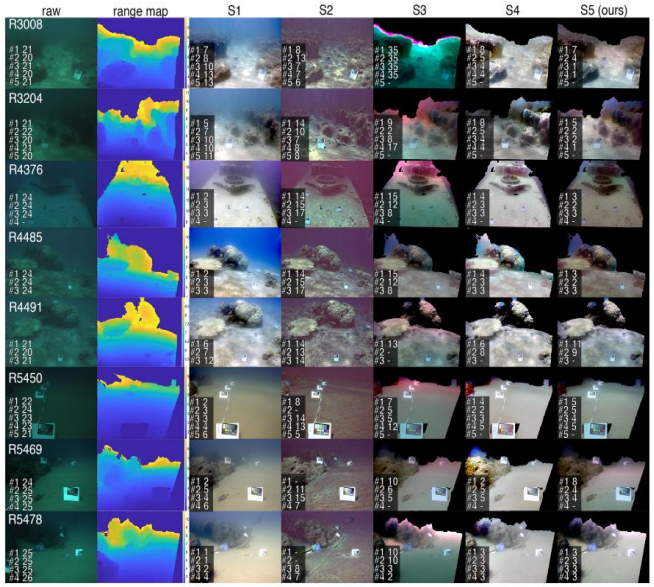

Figure 7. Results on the stereo dataset of [7]. Their range maps were further processed to remove spurious pixels. $\bar{\psi}$ rounded to the nearest integer is given in inset; chart #1 is closest to the camera. **S1** and **S2** do not utilize range maps; for others, lack of $\bar{\psi}$ values indicate missing range information. The average errors across all images are: **raw:** 22.28, **S1:** 6.83, **S2:** 10.03, **S3:** 12.04, **S4:** 4.46, **S5:** (*Sea-thru*) 4.94.

7. Conclusion

By suggesting improvements in the already existing image formation model, Sea-thru presents an opportunity to get better underwater images for mathematical or biological computations. It basically tells that β_c^D and β_c^B are different and that the z-dependency on β_c^D has to be considered. There is a focus on z-dependency because it is most prominent and we hope to tackle the ambient light dependency in the future. Also, better estimation techniques then the one used here can be used to improve the results. The dataset used here was acquired with the help of colour charts and is not always the best representation of the underwater scene.

Sea-thru is a large step towards the exploration of underwater world and will aslo help in the research at a time when our oceans are increasing stress from pollution, overfishing, and climate change.

Acknowledgments

The authors are grateful to Shailendra Tiwari for his guidance and Derya Akkaynak for her implementation of the Sea-thru method and for creating revised model for underwater imagery.

References

[1] D. Akkaynak and T. Treibitz. A revised underwater image formation model. In Proc. IEEE CVPR, 2018. 1, 2, 3, 4

[2] D. Akkaynak, T. Treibitz, T. Shlesinger, R. Tamir, Y. Loya, and D. Iluz. What is the space of attenuation coefficients in underwater computer vision? In Proc. IEEE CVPR, 2017. 2, 3, 4, 5

[3] C. Ancuti, C. O. Ancuti, C. De Vleeschouwer, R. Garcia, and A. C. Bovik. Multi-scale underwater descattering. In Proc. IEEE Int. Conf. on Pattern Recognition (ICPR), pages 4202–4207, 2016. 6

[4] C. O. Ancuti, C. Ancuti, C. De Vleeschouwer, and P. Bekaert. Color balance and fusion for underwater image enhancement. IEEE Trans. Image Processing, 27(1):379– 393, 2018. 6

[5] C. O. Ancuti, C. Ancuti, C. De Vleeschouwer, L. Neumann, and R. Garcia. Color transfer for underwater dehazing and depth estimation. In Proc. IEEE Int. Conf. Image Processing (ICIP), pages 695–699, 2017. 6

[6] S. Beigpour, C. Riess, J. Van De Weijer, and E. Angelopoulou. Multi-illuminant estimation with conditional random fields. IEEE Trans. Image Processing, 23(1):83–96, 2014. 5

[7] D. Berman, D. Levy, S. Avidan, and T. Treibitz. Underwater single image color restoration using haze-lines and a new quantitative dataset, 2018. 2, 3, 6, 8

[8] D. Berman, T. Treibitz, and S. Avidan. Non-local image dehazing. In Proc. IEEE CVPR, 2016. 2

[9] D. Berman, T. Treibitz, and S. Avidan. Diving into hazelines: Color restoration of underwater images. In Proc. British Machine Vision Conference (BMVC), 2017. 2, 3

[10] M. Bleier, C. Riess, S. Beigpour, E. Eibenberger, E. Angelopoulou, T. Troger, and A. Kaup. Color constancy and ¨ non-uniform illumination: Can existing algorithms work? In Proc. IEEE ICCVWorkshops, pages 774–781, 2011. 5

[11] D. L. Bongiorno, M. Bryson, and S. B. Williams. Dynamic spectral-based underwater colour correction. In Proc. MTS/IEEE OCEANS, 2013. 2

[12] M. Bryson, R. Ferrari, W. Figueira, O. Pizarro, J. Madin, S. Williams, and M. Byrne. Characterization of measurement errors using structure-from-motion and photogrammetry to measure marine habitat structural complexity. Ecology and Evolution, 7(15):5669–5681, 2017. 3

[13] M. Bryson, M. Johnson-Roberson, O. Pizarro, and S. B. Williams. True color correction of autonomous underwater vehicle imagery. J. Field Robotics, 2015. 2

[14] G. Buchsbaum. A spatial processor model for object colour perception. J. the Franklin institute, 310(1):1–26, 1980. 6

[15] J. Burns, D. Delparte, R. Gates, and M. Takabayashi. Integrating structure-from-motion photogrammetry with geospatial software as a novel technique for quantifying 3d ecological characteristics of coral reefs. PeerJ, 3:e1077, 2015. 3

[16] J. Burns, D. Delparte, L. Kapono, M. Belt, R. Gates, and M. Takabayashi. Assessing the impact of acute disturbances on the structure and composition of a coral community using innovative 3D reconstruction techniques. Methods in Oceanography, 15:49–59, 2016. 3

[17] N. Carlevaris-Bianco, A. Mohan, and R. M. Eustice. Initial results in underwater single image dehazing. In Proc. MTS/IEEE OCEANS, 2010. 2

[18] D. Cheng, D. K. Prasad, and M. S. Brown. Illuminant estimation for color constancy: why spatial-domain methods work and the role of the color distribution. JOSA A, 31(5):1049– 1058, 2014. 6

[19] J. Y. Chiang and Y.-C. Chen. Underwater image enhancement by wavelength compensation and dehazing. IEEE Trans. Image Processing, 21(4):1756–1769, 2012. 2

[20] J. Deng, W. Dong, R. Socher, L.-J. Li, K. Li, and L. Fei-Fei. ImageNet: A Large-Scale Hierarchical Image Database. In CVPR09, 2009. 1

[21] P. Drews, E. Nascimento, F. Moraes, S. Botelho, and M. Campos. Transmission estimation in underwater single images. In Proc. IEEE ICCV Underwater Vision Workshop, pages 825–830, 2013. 2, 6

[22] M. Ebner. Color constancy, volume 6. John Wiley & Sons, 2007. 5

[23] M. Ebner. Color constancy based on local space average color. Machine Vision and Applications, 20(5):283–301, 2009. 2, 6

[24] M. Ebner and J. Hansen. Depth map color constancy. BioAlgorithms and Med-Systems, 9(4):167–177, 2013. 5

[25] S. Emberton, L. Chittka, and A. Cavallaro. Underwater image and video dehazing with pure haze region segmentation. Computer Vision and Image Understanding, 168:145–156, 2018. 6

[26] R. Fattal. Dehazing using color-lines. ACM Trans. on Graphics (TOG), 34(1):13, 2014. 2

[27] R. Ferrari, D. McKinnon, H. He, R. N. Smith, P. Corke, M. Gonzalez-Rivero, P. J. Mumby, and B. Upcroft. Quantify- ´ ing multiscale habitat structural complexity: a cost-effective framework for underwater 3D modelling. Remote Sensing, 8(2):113, 2016. 3

[28] W. Figueira, R. Ferrari, E. Weatherby, A. Porter, S. Hawes, and M. Byrne. Accuracy and precision of habitat structural complexity metrics derived from underwater photogrammetry. Remote Sensing, 7(12):16883–16900, 2015. 3

[29] G. D. Finlayson, B. V. Funt, and K. Barnard. Color constancy under varying illumination. In Proc. IEEE ICCV, pages 720– 725, 1995. 5

[30] X. Fu, P. Zhuang, Y. Huang, Y. Liao, X.-P. Zhang, and X. Ding. A retinex-based enhancing approach for single underwater image. In Proc. IEEE Int. Conf. Image Processing (ICIP), pages 4572–4576, 2014. 5

[31] A. Galdran, A. Alvarez-Gila, A. Bria, J. Vazquez-Corral, and M. Bertalm´ıo. On the duality between retinex and image dehazing. In Proc. IEEE CVPR, pages 8212–8221, 2018. 5

[32] A. Gijsenij, T. Gevers, J. Van De Weijer, et al. Computational color constancy: Survey and experiments. IEEE Trans. Image Processing, 20(9):2475–2489, 2011. 5, 6

[33] K. He, J. Sun, and X. Tang. Single image haze removal using dark channel prior. In Proc. IEEE CVPR, 2009. 2

[34] K. He, J. Sun, and X. Tang. Single image haze removal using dark channel prior. Trans. IEEE PAMI, 33(12):2341–2353, 2011. 2, 6